Thermal Conductivity of the Damaged Gold Nanowires

Navin Kumar and Kishore Pochiraju
Design and Manufacturing Institute
& Mechanical Engineering Department
Stevens Institute of Technology,
Hoboken, New Jersey 07030, U.S.A.

Abstract

The damage propagation and the thermal conductivity of a gold nanowire are studied using molecular dynamics methods. The frequency spectra of stresses in the wire are also investigated for persistent features that correlate with bulk material behavior. The material is modeled using atomic scale representative volume elements with a finite dimension along one dimension and infinite dimensions in two others. The initial state temperature, pressure and volume states for the material are determined using a slow and sequential equilibrium procedure that produces a convergent energy and stress states. Finite size cracks surfaces are artificially created and the changes in the dynamic stress states are observed. The frequencies of the dominant modes and the amplitude of the stress at these modes are described. The shift in the frequency of the lowest dominant mode due to cracking and the increase in the concentration show some of the persistent features expected in the stress state due to the presence of a crack. At selected load steps the wire is mechanically equilibriated and thermal conductivity is measured. In order to measure the thermal conductivity a temperature gradient is established across a simulation domain by adding heat to one group of atoms (hot reservoir) and subtracting heat from another group of atoms (cold reservoir). Results are presented illustrats the thermal conductivity change behavior for a selected crack lengths.

## 1.	Introduction

The studies at the nanoscale with atomistic building blocks have been widely used in the past. Particularly, molecular dynamics (MD) methods are increasingly being used to study the mechanical behavior of nanostructures [1-3]. A continuum based model proposed by Griffith to predict the onset of crack growth in brittle material was based on equating the available strain energy to that required for creation of new crack surfaces. Early atomistic simulations of fracture were carried out by Ashurst and Hoover [4] in which they compared the free energies of finite element model and a bead-spring model in a triangular lattice. Later Abraham and coworkers [5] simulated the brittle fracture of a material using molecular dynamics models consisting of million atoms and with Lennard-Jones (LJ) inter-atomic potential. Zhou et al. [6] described fracture as the energy release by bond breakage which accumulates in a local phonon field and moves with the crack tip. Xu et al. [7] performed molecular dynamics simulation on ductile material and computed the virial stress field around the crack tip and its evolution during the crack growth.

Relating the virial stress computed from the atomistic scale to continuum stress has seen some controversy in the recent time. Different approaches were used to find stress measures

from atomistic simulations have been used. Basinski, et al. [8] based their calculation on a volumetric partition of the bulk homogeneous stress tensor. They have assumed that the bulk stress tensor which is valid for homogeneously deforming solids continues to characterize the stress state in a small volume about an atom even in an inhomogeneously deforming atomic assemblage. Hardy [9] used a finite-valued and finite-ranged localization function to define stress about an atom. While the range of this function and the characteristic size of the volume that contains atoms contributing to properties at the spatial point chosen can be selected arbitrarily, the resulting expression for stress contains terms that theoretically remain constant for different size volumes. Zimmerman et al. [10] reviewed Hardy's formalism and present a computational comparison between Hardy's expression for stress and local volume averages of the virial stress within a FCC crystal. Zhou [13] examined the virial stress and stated that it is not equivalent to the Cauchy stress if it contains both the kinetic and potential parts. Shen [11] and Sun [14] supported this view. However, Subramaniyan et al. [15] reiterated that virial stress is equivalent to Cauchy stress when properly averaged over space and time domains. Thermal conductivity of the material can be measured by standard molecular dynamics methods when the heat conduction is dominated by phonons. Both equilibrium molecular dynamics (EMD) and non equilibrium molecular dynamics (NEMD) methods can be used [18,19]. NEMD is a direct method that relies on imposing a temperature gradient across the simulation cell and is therefore analogous to the experimental situation, and thermal conductivity is simply evaluated as the ratio between the imposed heat flux and temperature gradient.

In this effort, we examine the fundamental modes in spatially averaged virial stress measures. We seek to compare the dynamic behavior of the stress states in the atomic ensemble with the bulk continuum behavior of an equivalent structure. In addition, we create a discrete crack which affects both the structural stiffness and the local stress states. In present study, non equilibrium molecular dynamics method is used to obtain thermal conductivity. Effect of the surfaces generated during crack growth on the thermal conductivity of the material is investigated. The rest of the paper describes the details for the simulations and the observations made in the time and frequency domain.

2. Simulations with Molecular Dynamics

2.1 Configurations

Molecular dynamics (MD) simulations with embedded atom method (EAM) potential are carried out. The atoms in the gold ensemble are arranged in a 4.08 Angstrom face centered cubic (fcc) lattice as shown in the Fig. 1. The model x, y and z axes are oriented along the [100], [010] and [001] crystalline directions, respectively. We consider a 20 cell x 40 cell x 20 cell domain with dimensions of 81.6 A x 163.2A x 81.6 A. There are 64800 atoms in the simulation domain. We assume that the model is periodic on the faces with normals along ±x and ±z and has finite boundaries at the faces with ±y boundary. The periodic boundary conditions allow the energy to flow though the boundary, while ensuring the conservation of momentum and energy, i.e. energy flow out of one surface will re-enter from other surfaces. On the finite boundary, the simulation box is moved to encompass the atoms along that dimension. The molecular dynamics simulations are carried out using LAMMPS MD package [20].
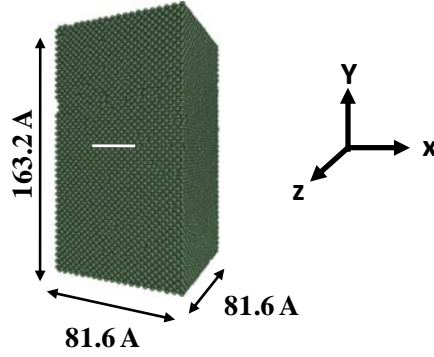
**Figure 1 Model used and dimension
parameters used in this analysis**

2.2 Interatomic potential and the virial stress measure

The embedded atom method (EAM), developed by Daw and Baskes [16, 17] taken as a model for bonding of fcc metals. The EAM potential consists of a many body term representing the interaction of an embedding atom core with the electronic charge density of the remaining atoms in the system and a pair wise term representing the electrostatic interactions between the atoms cores. The many body term is referred to as the embedding function. The total energy E of a system of N atoms can be written as

$$E_{total} = \sum_i^N \left(F_i(\bar{\rho}_i) + \frac{1}{2} \sum_{j \neq i}^N \phi_{ij}(r_{ij}) \right), \tag{1}$$

where ϕ_{ij} is the pair potential function between atoms i and j and r_{ij} is the distance between atom i and j, while F_i, the embedding term, is the quantum mechanical energy involving the influence of electron density. This term can be considered as the energy to embed an atom into an electron gas with a density i, which comes from the contributions of neighboring atoms. The electron density (ρ_i) term can be put as

$$\overline{\rho_i} = \sum_j^N \rho_j(r_{ij}) \tag{2}$$

where ρ_i depends only on the distance between two atoms. For a system of atoms in equilibrium state, the force that comes from embedding term is balanced with the force derived from pair wise interaction term. In the EAM potential developed by Voter and Chen [12] the atomic electron density is

$$\rho(r) = r^6(e^{-\beta_M r} + 2^9 e^{-2\beta_M r}) \tag{3}$$

where β_M is an adjustable parameter. The pair wise interaction is described by Morse pair potential

$$\phi(r) = D_M\{1 - e^{-\alpha_M(r-R_M)}\}^2 - D_M \tag{4}$$

where D_M, R_M, and α_M, respectively, are the depth of the potential, the distance to the minimum, and a measure of the curvature at the minimum. The value of D_M, R_M, and α_M, β, and the cutoff distances r_{cut} at which the function $\phi(r)$ and $\rho(r)$ and their derivatives are forced to go smoothly to zero. For metallic gold, the fitting parameters for Morse pair potential are r_{cut} (A) = 5.5155, β_M (1/A) =3.6967, α_M (1/A) =1.8964, D_M (eV) = 0.6748, R_M (A) = 2.5686.

Virial stress is an averaged measure of the interatomic force interactions of atoms with their neighboring atoms. In molecular simulation studies, virial stress averaged over the total volume

3

Ω is often found to be useful to study macroscopic material behavior to analyze stress distribution inside the system. The average virial stress is given as [13]

$$\overline{\sigma_{\iota J}} = -\frac{1}{\Omega}\sum_{\alpha=1}^{N^R}\left(m^\alpha v_i^\alpha v_j^\alpha - \frac{1}{2}\sum_{\beta\neq\alpha} f_i^{\alpha\beta} r_j^{\alpha\beta}\right) \qquad (5)$$

where, N^R is the number of atoms in the region. m^α is the mass, v_i^α is the i-th component of the velocity of atom α, $f_i^{\alpha\beta}$ is the i-th component of force between atom α and β; and $r_j^{\alpha\beta}$ is the j-th component of centre distance between atom α and β. It can be seen that that Eq. (5) represents average atomic stresses for the volume of the periodic box. Here, the first term is associated with the contribution from kinetic energy due to thermal vibration and the second term is related to change in potential energy due to applied deformation.

The thermal conductivity relates the heat current to the temperature gradient via Fourier's law as

$$q_\mu = -\sum_v \kappa_{\mu v}\left(\partial T / \partial x_v\right) \qquad (6)$$

Where q_μ is the thermal current, $\kappa_{\mu v}$ is an element of thermal conductivity tensor, and $\left(\partial T / \partial x_v\right)$ is the gradient of the temperature T.

3. Initial state determination

The gold crystal with infinite boundary condition in x and z directions and finite boundary condition in y direction [p s p], is heated from 0 K up to 250 K temperature. The gold lattice is first heated from 0 to 50K at 0.083K/ps heating rate for 600ps by using Nose-Hoover temperature thermostat and then it is equilibrated at this temperature for another 800ps (dwell) by using NVT conditions as shown in Fig. 2(a). This process of heating and equilibrium is repeated for every 50K rise in temperature until an equilibrium temperature of 250K is achieved. Although the mean pressure is observed to be low after equilibrating under NVT conditions, pressure fluctuations of 1500 bar can be observed. We further equilibrate the gold lattice by applying the NPT condition with a barostat set at 0.0001 bar and temperature held at 250K for another 3000ps.
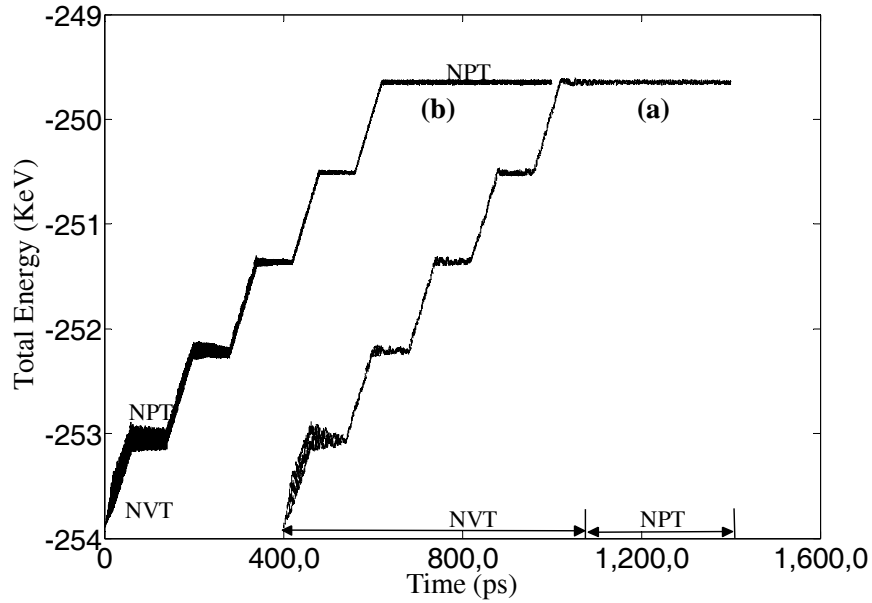
Figure 2 Case (a): Heating from 0-250K at NVT and then equilibrating at 250K by NPT; Case (b): Heating from 0-50K at NVT and then equilibrating at 50K by NPT condition and repeating this process for every 50K rise in temperature.

In another attempt to examine the effect of different equilibrium processes on the total energy, gold lattice is first heated at 0.083 K/ps under NVT condition for 600ps and then equilibrated under NPT condition for another 800ps at this temperature, shown as case (b) in Fig. 2. This heating at NVT and equilibration at NPT process is repeated till the system reaches a temperature of 250K. From the Fig. 2 it is evident the both systems attain the same total energy at the target temperature of 250K. The mean and standard deviation of pressure after NPT condition at 250K is 0 and 126 bar respectively

## 4. Frequency modes in virial stress at 250 ^{o}K

For case (a) after reaching the equilibrium stage the frequency spectrum of hydrostatic stress is plotted for last 2000ps as shown in Fig. 3. There are number of frequency peaks present in the frequency spectrum and the first frequency peak occur at 43 GHz.
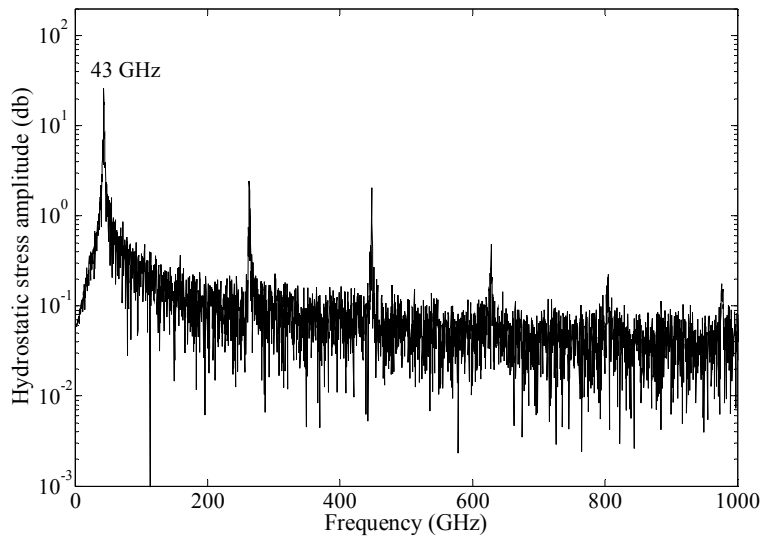
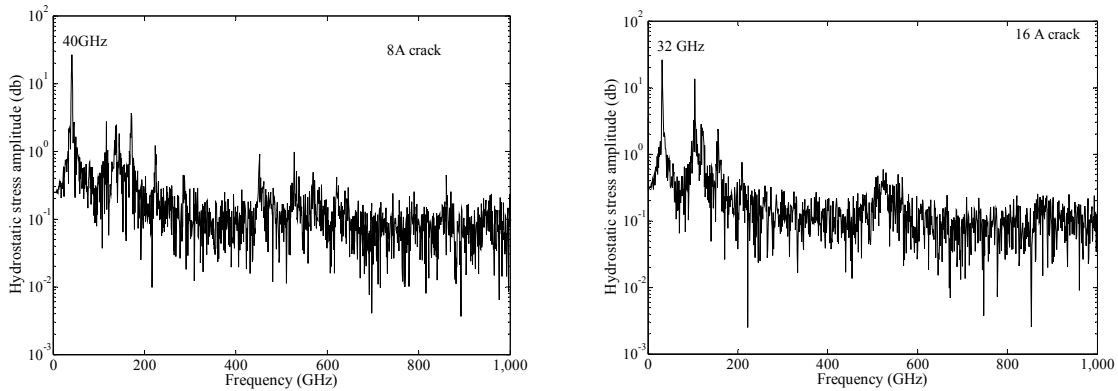**Figure 3 Spectrum response of the hydrostatic stress in gold lattice [81.6x163.2x81.6] A^3 without any crack.**

4.1 *Frequency response after crack initiation*

A discrete crack is created in the middle of the lattice by removing the pair-wise interactions between atoms on both sides of the crack plane. After the crack initiation, the gold lattice is equilibrated for another 2000ps under NPT conditions. Separate simulations are run for gold lattice with 8A and 16A crack length. The total energies of the system with 8A and 16A crack lengths are shown in Fig. 4. The difference in the energy level is attributable to the presence of crack surfaces and is seen to be proportional to the area of new surfaces introduced into the model.
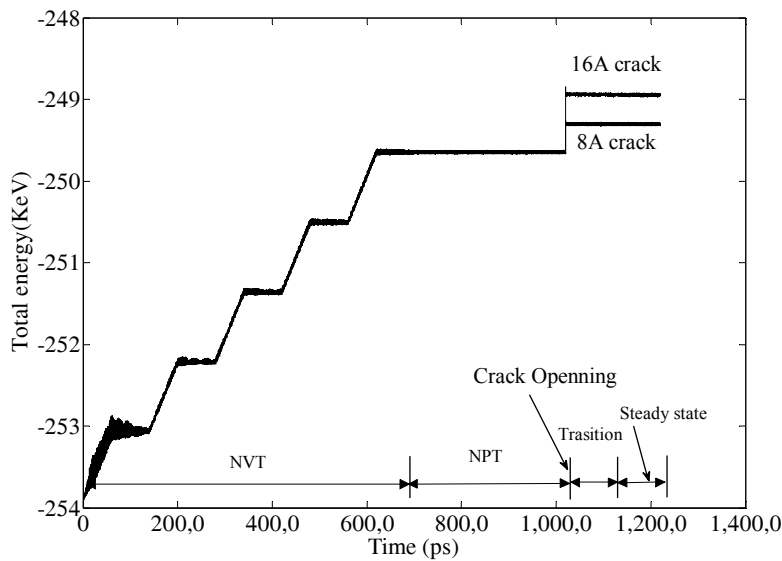
Figure 4 Equilibrium process before and after crack opening

The fundamental mode of vibration determined form the simulation is seen at 43GHz before initiation of the crack. This dominant mode shifts to 40 GHz for the model with 8A crack as shown in Fig. 5. This shift may be attributed to the change in the stiffness of the structure due to the introduction of the crack in the model. Increasing the size of the crack to 16A reduces the frequency of the fundamental mode to 32 GHz consistent with further reduction in the stiffness of the model.

Figure 5 Spectral responses of the hydrostatic stress in gold lattice [81.6x163.2x81.6] A^3 with 8A and 16 A cracks.

5. Thermal transport in damaged continua

In order to test the thermal conductivity of the gold lattice, a temperature gradient is created by non-translational kinetic energy (heat) to one group of atoms (hot reservoir) and subtracting from another (cold reservoir). Heat addition/subtraction is performed every 0.01ps. Heat flux, Q, is determined by the change in the aggregate energy of the entire group of atoms. Fig. 6 shows the temperature behavior of the hot and cold surfaces for uncracked and cracked models The temperature gradient is higher for the model with 10A crack compared to the uncracked model showing reduction in the thermal conductivity. The crack size is then varied from 2A to 10A in length and the thermal conductivity is measured. Fig. 7 shows that the reduction in the thermal conductivity in comparison with the uncracked case. Nearly 30% decrease in the conductivity is seen with a 10A crack.
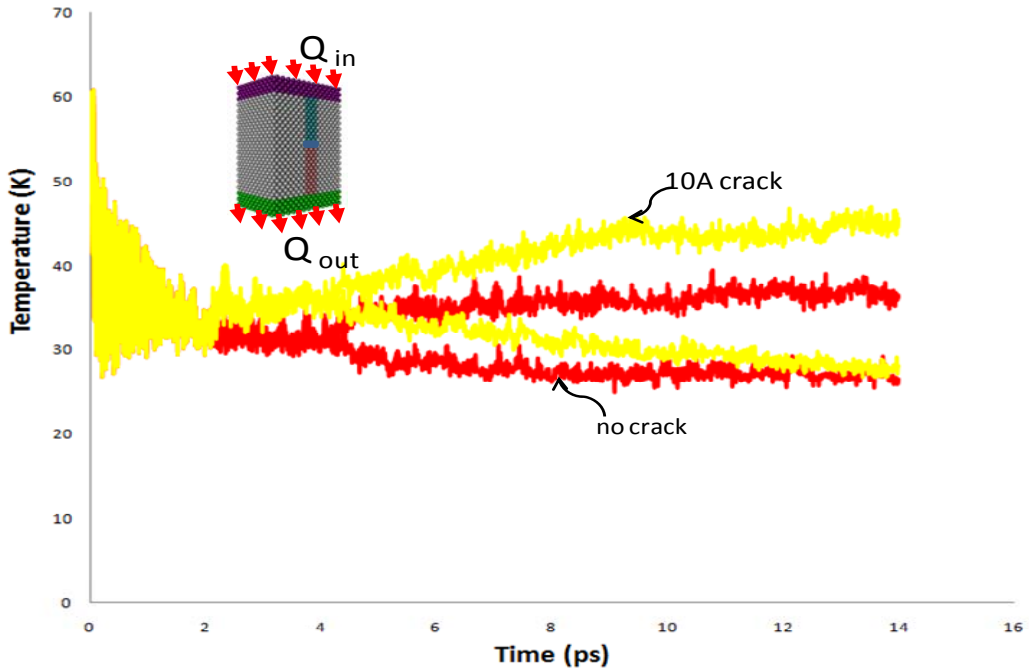
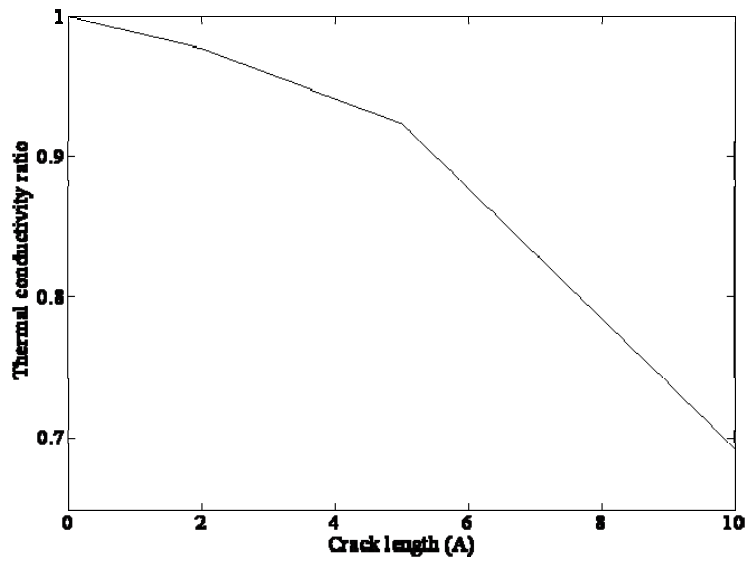**Figure 6 Temperature gradient without any crack and with 10A crack length**

Figure 7 Thermal conductivity with different size of crack lengths

6.   Concluding remarks

Whether virial stress is a representation of Cauchy stress has been questioned in the recent times. Zhou [13] has concluded that the virial stress is not an equivalent of Cauchy stress and only potential energy component of virial stress is relevant. Subramaniyan and Sun [15] stated that the properly averaged virial stress in time and space represent the Cauchy stress and showed that bulk thermal expansion coefficients and thermally induced stresses can be correlated with virial stress measures. However, the stress components used in both these studies have been averaged spatially as well as temporally. This promulgates the perspective that the temporal fluctuation in the states are random instances about a mean state and correlate to neither the spatial variations nor the structural vibration states. In this effort, we investigate the dynamics of hydrostatic stress computed and observe the changes in the lowest dominant mode. We note that some fundamental modes are persistant in the dynamical stress states and have similarities to structural vibration modes. In this study a complete correlation with structural modes has not been presented and will be elucidated in near future. Furthermore, we initiate a discrete crack in the atomistic model and study its effect on both the fundamental modes and the amplitude of the virial stress. The shift in fundamental mode which is consistent with decrease in stiffness indicate that the stress behavior consistent that observed in bulk stress fields.

Next we examined the effect of opening the discrete crack on the thermal conductivity. Thermal conductivity of the gold lattice significantly reduces due to presence of the crack. The reduction in thermal conductivity with the crack length is parametrically determined using molecular dynamics methods.

References

1. Komanduri R., Chandrasekaran N. and Raff L. M., Molecular Dynamics Simulation of Uniaxial Tension of Some Single Crystal Cubic Metals at Nanolevel, *Int. J. Mechanical Sciences,* 2001, 43, 2237.
2. Diao J., Gall K., and Dunn M. L., Yield Strength Asymmetry in Metal Nanowires, *Nano Letters* 4(10), 2004, 1863–1867.
3. Gall K., Diao J., and Dunn M. L., The Strength of Gold Nanowires *Nanoletters, 2004* 4(12), 2431.
4. Ashurst W. T. and Hoover W. G., Microscopic Fracture Studies in the Two-Dimensional Triangular Lattice, *Physical Review B*, 1976 14(4), 1465-1473.
5. Abraham F. F., Brodberk D., Rafey R. A. and Rudge W. E., Instability Dynamics of Fracture: A Computer Simulation Investigation, *Phys. Rev. Lett.,* 1994 73(2), 272-275.
6. Zhou S. J., Lomdahl P. S., Thomas R., and Holian B. L., Dynamic Crack Process via Molecular Dynamics, *Phys. Rev. Lett.,* 1996 76(13), 2318-2321.
7. Xu S. and Deng X., Nanoscale Void Nucleation and Growth and Crack Tip Stress Evolution ahead of a Growing Crack in a Single Crystal, *Nanotechnology,* 2008(19), 115705.
8. Basinski Z. S., Duesbery M. S. and Taylor R., Influence of Shear Stress on Screw Dislocations in a model Sodium Lattice, *Can. J. Phys*. 49, 2160, 1971.

9. Hardy R J and Karo A M , Stress and Energy Flux in the Vicinity of a Shock Front *Shock Compression of Condensed Matter: Proc. American Physical Society Topical Conf.* (North Holland: Amsterdam, Netherlands) 161–4, 1990.
10. Zimmerman J A, Webb E B, Hoyt J J, Jones R E, Klein P A, Bammann D J, Calculation of Stress in Atomistic Simulation, *Modelling Simul. Mater. Sci. Eng.* 12 2004.
11. Shen S., Atluri, S.N., 2004. Atomic-level Stress Calculation and Continuum-MolecularSystem Equivalence, *Computer Modeling in Engineering and Sciences* 6**,** 91-104.
12. Voter A. F. and Chen S. P., Characterization of Defects in Materials, *Mater. Res. Soc. Symp. Proc. No.*82 (Material Research Society, Pittsburgh, 1987), 175.
13. Zhou M., A New Look at the Atomic Level Virial Stress-on Continuum-Molecular System. Equivalence, *Proc. R. Soc. London A*, 2003 459, 2347-2392.
14. Sun, Z.H., Wang, X.X., Wu, A.K.S.H.A., On stress calculations in atomistic simulations. *Modelling and Simulation in Materials Science and Engineering* 14**,** 423-431.
15. Subramaniyan A.K. and Sun C.T., Continuum Interpretation of Virial Stress in Molecular Simulations, *International Journal of Solids and Structures, in press* (2008).
16. Daw M. S. and Baskes M. I., Semi empirical, Quantum Mechanical Calculation of Hydrogen Embrittlement in Metals, *Phys Rev. Lett,* 1983 50(17), 1285.
17. Daw M. S. and Baskes M. I., Embedded-Atom Method: Derivation and Application to Impurities and other Defects in Metals, *Phys Rev. B,* 1984 29, 6443.
18. Schelling P.K, Phillpot S.R. and Keblinski P., Comparison of atomic-level simulation methods for computing thermal conductivity, *Physical Review B*, vol 65, 144306
19. Tretiakov K. V.Thermal conductivity of solid argon from molecular dynamics simulations, *Journal of Chemical Physics*, vol.120, 8.
20. Plimpton S., Fast parallel algorithms for short-range molecular dynamics, *J. Comput. Phy*. 117 1-19.